ADVANCED SUSTAINABLE SYSTEMS
www.advsustainsys.com

A Triad Photoanode for Visible Light-Driven Water Oxidation via Immobilization of Molecular Polyoxometalate on Polymeric Carbon Nitride

Ruihao Gong, Dariusz Mitoraj, Dandan Gao, Manuel Mundszinger, Dieter Sorsche, Ute Kaiser, Carsten Streb, Radim Beranek, and Sven Rau**

Due to their availability, low cost, nontoxicity, and tunability, polymeric carbon nitrides (CN_x) represent one of the most attractive materials classes for the development of fully sustainable photo(electro)catalytic systems for solar-driven water splitting. However, the development of CN_x-based photoanodes for visible light-driven water oxidation to dioxygen is rather challenging, particularly due to issues related to photoelectrode stability and effective coupling of the light absorber with water oxidation catalysts. Herein, a triadic photoanode comprising a porous TiO_2 electron collector scaffold sensitized by CN_x coupled to a molecular cobalt polyoxometalate (CoPOM = $[Co_4(H_2O)_2(PW_9O_{34})_2]^{10-}$) catalyst is reported. Complete water oxidation to dioxygen under visible ($\lambda > 420$ nm) light irradiation is demonstrated, with photocurrents down to relatively low bias potentials (0.2 V vs RHE). Furthermore, polyethyleneimine (PEI), a cationic polymer is shown to act as an effective and non-sacrificial electrostatic linker for immobilization of the anionic CoPOM onto the negatively charged surface of CN_x. The optimized deposition of CoPOM using the PEI linker translates directly into improved efficiency of the transfer of photogenerated holes to water molecules and to enhanced oxygen evolution. This work thus provides important design rules for effective immobilization of POM-based catalysts into soft-matter photoelectrocatalytic architectures for light-driven water oxidation.

1. Introduction

Solar-driven water splitting utilizing photo(electro)catalytic systems is a possible strategy to secure the future supply of low-entropy energy in form of storable high-energy molecular fuels, such as hydrogen, alcohols, or hydrocarbons.[1–5] However, practically viable and sustainable systems required for large-scale applications should be preferably based on highly abundant and low-cost materials with non-critical availability, i.e., without any possible supply restrictions due to various political, economic or environmental concerns. In terms of sustainability, low cost, and non-toxicity, one of the most attractive materials for photo(electro)catalytic applications are polymeric carbon nitrides (CN_x).[6–9] Carbon nitrides are readily available, tunable and chemically robust polymers,[10] that have been widely utilized in a variety of light-driven chemical processes such as hydrogen evolution,[11–14] CO_2 reduction,[15,16] selective chemical syntheses,[17–20] or organic pollutants degradation.[21,22] However, the studies demonstrating visible light-driven water oxidation to dioxygen using CN_x-based photoelectrocatalytic systems are still rather rare.[23,24] This is, on the one hand, due to the notoriously slow kinetics of the oxygen evolution reaction (OER),[25] which typically results in accumulation of oxidizing equivalents that translates into enhanced photocorrosion of CN_x.[26] On the other hand, the very fabrication of mechanically robust CN_x-based photoelectrodes is challenging,[27,28] in particular due to the poor adhesion of CN_x to conductive substrates,[29–32] and the very low conductivity of CN_x films, hindering efficient charge transport to the external circuit.[33]

In our own work, we have been developing a distinct type of hybrid CN_x-based photoanodes in which a thin layer of CN_x is deposited onto a porous TiO_2 layer that acts as an electron-collecting scaffold, overcoming thus at the same time both the problems of low adhesion and low electronic conductivity of CN_x. Such photoanodes are capable of visible light-driven oxygen evolution upon deposition of a suitable cocatalyst for water oxidation, typically in form of metal oxide (IrO_x, CoO_x, NiO_x) nanoparticles.[26,34–41] Notably, we found out that one of the crucial problems of the metal oxide nanoparticles as cocatalysts is their parasitic absorption of visible light, blocking thus the light

R. Gong, D. Gao, D. Sorsche, C. Streb, S. Rau
Institute of Inorganic Chemistry I
Ulm University
Albert-Einstein-Allee 11, 89081 Ulm, Germany
E-mail: sven.rau@uni-ulm.de
D. Mitoraj, R. Beranek
Institute of Electrochemistry
Ulm University
Albert-Einstein-Allee 47, 89081 Ulm, Germany
E-mail: radim.beranek@uni-ulm.de
M. Mundszinger, U. Kaiser
Electron Microscopy Group of Materials Science
Ulm University
Albert-Einstein-Allee 11, 89081 Ulm, Germany
The ORCID identification number(s) for the author(s) of this article can be found under https://doi.org/10.1002/adsu.202100473.

© 2022 The Authors. Advanced Sustainable Systems published by Wiley-VCH GmbH. This is an open access article under the terms of the Creative Commons Attribution License, which permits use, distribution and reproduction in any medium, provided the original work is properly cited.

DOI: 10.1002/adsu.202100473

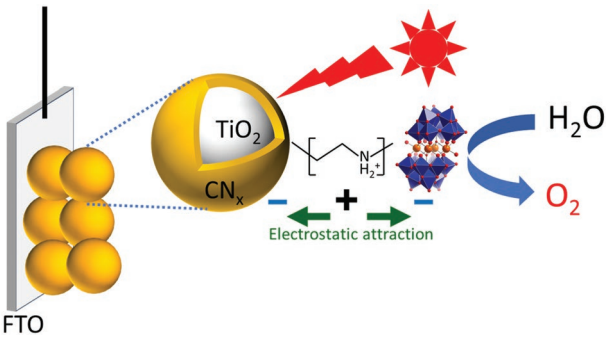

Scheme 1. The fabrication of the CN_x/TiO_2 hybrid photoanode with an anionic molecular CoPOM cocatalyst immobilized via electrostatic attraction on the negatively charged CN_x surface using a positively charged cationic PEI linking agent.

absorption by the light absorber. This problem could be only partially overcome by using, for example, ultrasmall (1–2 nm) $CoO(OH)_x$ nanoparticles that exhibit a larger bandgap and correspondingly better transparency in the visible range due to quantum size effects.[26] This led us to hypothesize that, in contrast to conventional bulk metal oxide-based water oxidation catalysts, a *molecular*-scale catalyst might be favorable for preventing the undesired light absorption by the catalyst and enabling also more controllable cocatalyst deposition. With this motivation in mind, we turned our attention to water oxidation catalysts based on well-defined molecular polyoxometalates (POMs), such as $[Co_4(H_2O)_2(PW_9O_{34})_2]^{10-}$ = CoPOM, a tetra-cobalt-doped polyoxometalate, that have attracted much attention with regards to catalytic applications,[42–46] and have been previously utilized as cocatalysts on various semiconducting metal oxides (e.g., TiO_2, Fe_2O_3) to fabricate photoanodes for light-driven water splitting.[47,48] However, to the best of our knowledge, no studies on CN_x-based photoanodes comprising molecular POMs cocatalysts for photoelectrocatalytic water-splitting have been reported so far.

Herein, we report for the first time a triadic design of a photoanode consisting of porous TiO_2 as an electron collector, CN_x as a sensitizer for visible light, and CoPOM as a molecular water oxidation catalyst. The triad photoanode enables visible ($\lambda > 420$ nm) light-driven oxidation of water to dioxygen at moderate bias potentials (>0.2 V vs RHE). Notably, we show that effective immobilization of CoPOM into the porous structure of the photoanode plays a crucial role in photoanode performance and can be significantly improved using polyethyleneimine (PEI), a cationic polymer that can act as a non-sacrificial, electrostatic linker between the surface of CN_x and the CoPOM that are both charged negatively (**Scheme 1**). The thus achieved optimized immobilization of CoPOM is demonstrated to result in a more efficient transfer of photogenerated holes to water molecules and enhanced oxygen evolution.

2. Experimental Section

2.1. Materials

Fluorine-doped tin oxide (FTO) Pilkington TEC glass was purchased from the XOP company (XOP Glass, Castellón Spain). Deionized water was used for rinsing samples. TiO_2 powder (Hombikat UV 100, Sachtleben, Germany, anatase, specific surface area (BET) ≈ 300 $m^2\ g^{-1}$, crystallite size < 10 nm) was used to prepare the substrate for CN_x deposition. Urea, PEI (50 wt%, dissolved in water), anhydrous ethanol, 2-propanol, acetone, sodium hydroxide, boric acid (99.5%), sodium sulfite, and hydrochloric acid (37%) were purchased from Sigma–Aldrich, $Na_2WO_4 \cdot 2H_2O$, $Na_2HPO_4 \cdot 7H_2O$, NaCl, and $Co(NO_3)_2 \cdot 6H_2O$ were provided by Merck.

2.2. Synthesis of CoPOM

The CoPOM complex was synthesized according to literature.[42] Briefly, $Na_2WO_4 \cdot 2H_2O$ (50.89 g), $Na_2HPO_4 \cdot 7H_2O$ (4.60 g) and $Co(NO_3)_2 \cdot 6H_2O$ (9.98 g) were dissolved in 50 mL deionized water in a 200 mL round-bottom flask. The pH was adjusted to 7 by HCl under magnetic stirring. The solution was then stirred and refluxed at 100 °C for 2 h and cooled down to room temperature. CoPOM was finally obtained by recrystallization and washed by deionized water. The purity of CoPOM is confirmed by Attenuated total reflection Fourier transform infrared (ATR-IR) spectroscopy.

2.3. Preparation of FTO/TiO_2 Substrates

TiO_2 layers on FTO were prepared using an established doctor-blading protocol.[26] Briefly, 0.25 g TiO_2 powder (Hombikat UV-100, pure anatase) was added to 1.25 mL anhydrous ethanol. The mixture was treated in ultrasonic bath for 10 min to produce a well-dispersed suspension. The FTO glass substrates with a size of 1.5 × 2.5 cm were first cleaned by acetone for removing residual organic contaminants by ultrasonication for 20 min. The cleaned FTO glass was then etched in 0.1 M NaOH and rinsed with deionized water. Two FTO glass pieces were placed between microscope glasses and fixed using a 3M scotch tape as frame and spacer, leaving an exposed area of ≈1.5 × 1.5 cm. Then, 200 µL TiO_2 suspension was dropped on the microscope glass and gently swept by a glass stick onto the FTO glass pieces. After drying at 70 °C for 20 min, the TiO_2 films were pressed at 10^4 N to improve the mechanical stability. All samples were calcined at 450 °C for 30 min in air before any tests or further treatments. The FTO/TiO_2 substrates were abbreviated as TiO_2 in this report.

2.4. Deposition of CN_x

CN_x was deposited by chemical vapor deposition of urea pyrolysis products according to the previous report.[26] Two pieces of TiO_2 electrodes were placed in a Schlenk tube connected to a round-bottom flask containing 1 g of urea. Before the CN_x deposition was started, the muffle oven (Carbolite, Germany) was preheated to 425 °C. Then, the reactor was directly placed into the muffle oven and heated at 425 °C for 30 min. Finally, the reactor was cooled down to room temperature in air. The resulting electrodes are denoted as CN_x-TiO_2.

2.5. Immobilization of CoPOM on CN_x-TiO_2

First, CoPOM (5×10^{-3} M) and PEI (6×10^{-3} M, based on monomer) solutions in an aqueous solution of sodium phosphate

© 2022 The Authors. Advanced Sustainable Systems published by Wiley-VCH GmbH

(80×10^{-3} M, pH 5) and NaCl (137×10^{-3} M) were prepared. Then, CN_x-TiO_2 electrode was first dipped into the PEI solution for 5 min, then rinsed with distilled water and dried in air, followed by dipping in the CoPOM solution for another 5 min. The dipping processes in PEI and CoPOM were alternately repeated for five times to acquire desired amount of CoPOM and the sample was named as CoPOM-PEI-CN_x-TiO_2. The reference sample without PEI was prepared by dipping CN_x-TiO_2 only into the CoPOM solution for five times and named as CoPOM-CN_x-TiO_2

2.6. Material Characterization

The electronic absorption spectra were measured using a UV–vis spectrophotometer (UV-2600, Shimadzu, Japan) equipped with the integrating sphere and the absorptance (Abs.) was calculated by the equation:

$$\text{Absorptance}(\%) = 100\% - \text{Reflectance}(\%) - \text{Transmittance}(\%) \quad (1)$$

The baselines were recorded using an FTO glass and a $BaSO_4$ plate as references for transmittance and reflectance, respectively. Scanning electron microscopy (SEM) and focused Ga ion beam (FIB) cross sections were performed using a NVision 40 Ar (Carl Zeiss Microscopy, Germany) SEM/FIB crossbeam machine. energy-dispersive X-ray spectroscopy (EDX) investigations were done with the attached Octane Elite (AMETEK EDAX, USA) EDX system. Photoluminescence (PL) spectra were recorded on an RF-6000 spectrofluorophotometer (Shimadzu, Japan) using excitation wavelength of 360 nm with a 400 nm cut-off filter placed in front of the emission detector. ATR-IR spectroscopy was performed by the FT-IR spectrometer (Alpha II, Bruker, Germany). X-ray photoelectron spectroscopy (XPS) measurements were performed with monochromatized Al Kα radiation using a PHI Quantera SXM system (ULVAC-PHI, Japan). The binding energies were calibrated based on C 1s peak of adventitious carbon (284.8 eV).

2.7. Photoelectrocatalytic Measurements

The photoelectrochemical measurements were conducted using an SP-300 BioLogic potentiostat and a typical 3-electrode system consisting of a Pt wire counter electrode, a Ag/AgCl (3.5 M KCl, 0.207 V vs SHE) reference electrode and tested photoanodes as working electrodes with geometric irradiation area of 0.5 cm^2. Photoanodes were irradiated by visible light ($\lambda > 420$ nm) using a 150 W Xe lamp (L.O.T.-Oriel) with light power density of ≈150 mW cm^{-2}, equipped with a KG-3 (LOT-Quantum Design) heat-absorbing filter and a 420 nm longpass optical filter. All electrodes were illuminated from backside (through FTO glass). All photoelectrochemical measurements at hybrid photoanodes were carried out at least in triplicate (at three different electrodes), and representative average data is shown.

The charge separation efficiency (η_{sep}) and the hole transfer efficiency (η_{tr}) were evaluated using the approach reported by Dotan et al.,[49] and utilizing sodium sulfite as a readily oxidizable reducing agent.[50] The hole transfer efficiency (η_{tr}) was determined using the equation:

$$\eta_{tr} = J_{H_2O}/J_{Na_2SO_3} \quad (2)$$

where J_{H_2O} and $J_{Na_2SO_3}$ are the photocurrents measured in the absence and presence of additional hole scavenger (Na_2SO_3), respectively. The charge separation efficiency (η_{sep}) was estimated by the equation:

$$\eta_{sep} = J_{Na_2SO_3}/J_{max} \quad (3)$$

where J_{max} is the maximal photocurrent obtained by integrating the Abs spectrum (**Figure 1**b) over the AM1.5G solar spectrum (ASTM G-173;[51] 1.5 sun intensity) from 420 to 600 nm with Abs at 600 nm as a baseline.

The oxygen evolution was recorded by the FireSting optical fiber oxygen meter (PyroScience, GmbH) in a home-made air-tight two-compartment cell with the oxygen collection efficiency as ≈75%, which was estimated by a direct electrolysis using a Pt working electrode. The volume of the photoanode compartment was 5 mL. The oxygen concentrations were not corrected for the losses in the gaseous headspace. The electrolyte was purged with argon before the electrodes were illuminated under applied potential of 1.12 V versus RHE. The incident monochromatic photon-to-current conversion efficiency (IPCE) was recorded using a photoelectric spectrometer

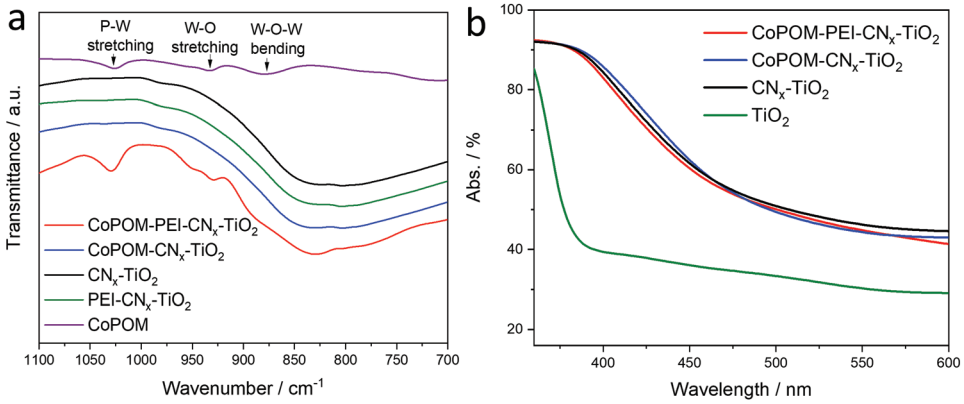

Figure 1. ATR-FTIR spectra of all CN_x-containing electrodes and CoPOM powder a); UV–vis electronic absorption spectra of the photoanodes; Abs., absorptance b). The nonzero baseline can be ascribed to the differences in internal reflection and scattering at the FTO/TiO_2 interface in the transmittance and reflectance measurement modes.[57]

© 2022 The Authors. Advanced Sustainable Systems published by Wiley-VCH GmbH

(Instytut Fotonowy Sp. z o.o.) equipped with a tunable monochromatic light source provided with a 150 W Xenon lamp and a grating monochromator with a bandwidth of ≈10 nm. The value of photocurrent density was the difference between current density under irradiation and in the dark in steady-state conditions with a wavelength sampling interval of 10 nm. The IPCE value for each wavelength was calculated according to equation:

$$IPCE(\%) = \left(i_{ph}hc\right) / \left(\lambda Pq\right) \times 100\% \quad (4)$$

where i_{ph} is the photocurrent density, h is Planck's constant, c is the velocity of light, P is the light power density, λ is the irradiation wavelength, and q is the elementary charge. The electrolyte for all photoelectrochemical measurements was 0.1 M sodium borate electrolyte with pH value of 8.0. Na_2SO_3 (0.1 M) was dissolved in the electrolyte when photocurrents were measured in the presence of sacrificial electron donor. All potentials are recalculated and reported versus RHE.

3. Results and Discussion

The immobilization of the negatively charged $[Co_4(H_2O)_2(PW_9O_{34})_2]^{10-}$ (CoPOM) water oxidation catalyst onto polymeric carbon nitride is challenging since the surface of carbon nitride is known to be negatively charged due to large amount of unprotonated surface Brønsted base moieties that can be protonated only by highly concentrated strong acids.[52,53] In order to effectively immobilize the anionic CoPOM cocatalyst onto the internal surface of our porous CN_x-TiO_2 photoelectrodes, we have therefore utilized the layer-by-layer technique demonstrated by Jeon et al. for immobilization of CoPOM onto various metal oxides.[47] The CN_x-TiO_2 electrodes carrying a negative surface net charge were sequentially immersed into a solution of the cationic PEI and a solution of the anionic CoPOM for the desired number of times to fabricate the CoPOM-PEI-CN_x-TiO_2 photoanode. It is known that PEI can be protonated in a wide pH range (pH 3–10) when dissolved in aqueous solutions.[54] The positively charged cationic PEI thus plays a role of an electrostatic linker between CN_x and CoPOM that are both charged negatively. For comparison, the CN_x-TiO_2 electrodes were also only dipped into the CoPOM solution resulting in the reference, linker-free electrodes CoPOM-CN_x-TiO_2. To evaluate and compare the CoPOM loading of the two CoPOM-containing CN_x-TiO_2 electrodes, energy dispersive X-ray (EDX) spectra were recorded. The CoPOM-PEI-CN_x-TiO_2 electrode shows significantly higher concentration of elements contained in CoPOM, with 0.35 at% Co, 0.13 at% P, and 0.97 at% W, compared to 0.05 at% Co, 0.07 at% P, and 0.03 at% W in case of the PEI-free CoPOM-CN_x-TiO_2 reference electrode (Figure S1, Supporting Information). The higher CoPOM loading of CoPOM-PEI-CN_x-TiO_2 was further corroborated by XPS, showing the increase of surface concentration of Co by the factor of 3.4 in photoelectrodes comprising the PEI linker (Figure S2, Supporting Information). In addition, the EDX mapping analysis (Figures S3–S6, Supporting Information) shows the presence of CoPOM within the whole volume of the porous CN_x-TiO_2 film and confirms that the CoPOM loading and the homogeneity of its distribution throughout the whole thickness of the CN_x-TiO_2 porous film is enhanced in the presence of the PEI linker. Finally, only in the case of CoPOM-PEI-CN_x-TiO_2, the characteristic IR fingerprint of CoPOM[42] is detectable (Figure 1a), which confirms improved CoPOM immobilization compared to electrodes without the cationic PEI linker. Hence, we conclude that the more effective immobilization of CoPOM in the CoPOM-PEI-CN_x-TiO_2 photoanodes is due to beneficial effect of the electrostatic attraction between the positively charged PEI linker and the negatively charged CN_x and CoPOM components.

Figure 1b depicts the UV–vis electronic absorption spectra of TiO_2, CN_x-TiO_2, CoPOM-CN_x-TiO_2, and CoPOM-PEI-CN_x-TiO_2. All CN_x-containing electrodes exhibit a significant red shift compared to the optical absorption of pristine anatase TiO_2 (3.2 eV, ≈390 nm) and CN_x (2.9 eV, ≈428 nm), which we ascribe to effective sensitization of TiO_2 by CN_x, including formation of a charge-transfer complex between CN_x and TiO_2, making thus possible also the direct optical electron transfer from the HOMO of CN_x to the conduction band of TiO_2.[55] The optical absorption edge of the hybrid photoanodes (≈2.6 eV, ≈477 nm) determined from the Tauc plots (Figure S7, Supporting Information) is larger than the value typically obtained in our previous studies (≈2.3–2.5 eV),[26,34–40] which can be explained by the inherent limitations of the Tauc formalism as applied for bandgap determination of hybrid materials,[56] and to the fact that in previous studies we determined the bandgap using the Kubelka–Munk function calculated from diffuse reflectance spectra of corresponding powders, while here we use Abs data obtained from measurements on complete photoanodes. Notably, the change in electronic absorption properties upon the deposition of the CoPOM catalyst is negligible, which indicates that the parasitic light absorption by the CoPOM catalyst is very low. This clearly highlights the advantage of using the molecular CoPOM as compared to, for example, cobalt oxide catalysts that typically show significant light absorption in the visible range due to their fully developed band structure and correspondingly low bandgap, blocking thus partially the visible light absorption by the light absorber.[35]

The photoelectrocatalytic properties of our photoanodes were investigated under visible light ($\lambda > 420$ nm) using an appropriate cutoff-filter, in order to effectively shut off the intrinsic UV light absorption of TiO_2. The porous TiO_2 layer thus serves solely as an electron-collecting scaffold that transports electrons injected under visible light irradiation from CN_X into TiO_2 to the underlying FTO glass support, whereas the oxidizing equivalents (i.e., photoholes) photogenerated in CN_x should be ideally channeled to the water-oxidizing CoPOM catalyst to drive dioxygen evolution from water. First, potential-dependent photocurrents (**Figure 2**a) were measured for all electrodes utilizing illumination by chopped visible light ($\lambda > 420$ nm, 150 mW cm^{-2}) in borate electrolyte (pH 8). As expected, no photocurrents could be detected at the pristine TiO_2 substrate since anatase TiO_2 cannot be excited by visible light. The photocurrents recorded for the CN_x-TiO_2 electrode without any CoPOM catalyst are attributed to the photocorrosion processes presumably at the CN_x/TiO_2 interface as no oxygen evolution was detected at this electrode under identical experimental conditions (see Figure 4). In contrast, the photocurrent values significantly

© 2022 The Authors. Advanced Sustainable Systems published by Wiley-VCH GmbH

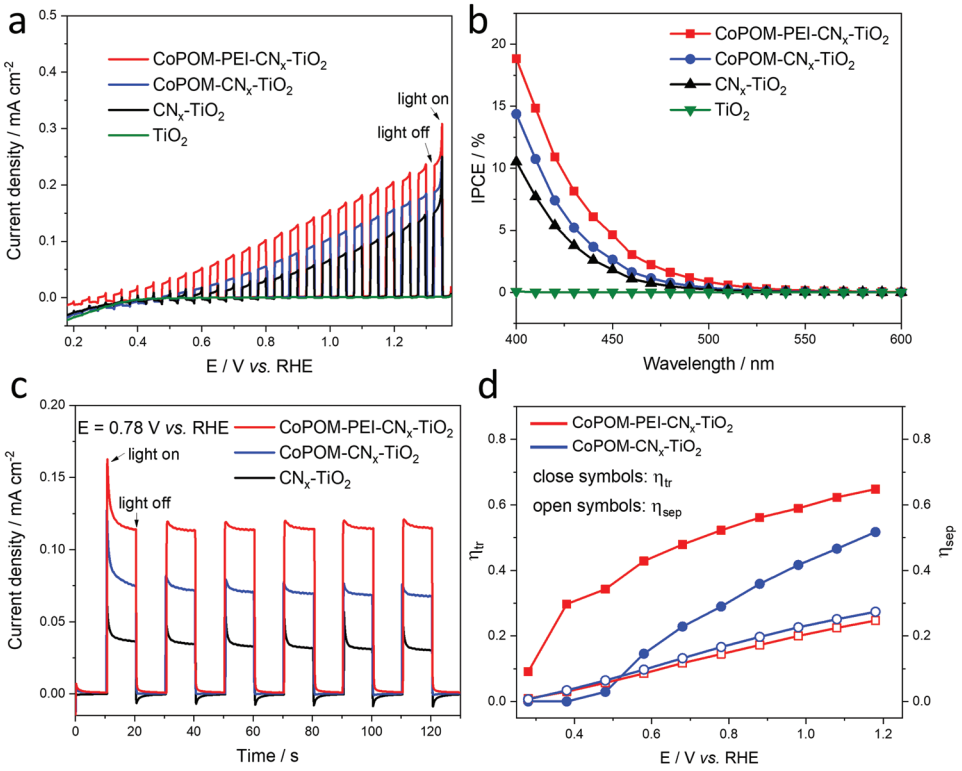

Figure 2. Photocurrents recorded under intermittent polychromatic visible light ($\lambda > 420$ nm) in borate electrolyte (0.1 M, pH 8.0) at cathodic sweep of 5 mV s^{-1} a); IPCE spectra under intermittent monochromatic irradiation measured at 1.12 V versus RHE in borate electrolyte (0.1 M, pH 8.0) b); photocurrent transients recorded under intermittent polychromatic visible light ($\lambda > 420$ nm, 150 mW/cm^{-2}) in borate electrolyte (0.1 M, pH 8.0) at 0.78 V versus RHE c); hole transfer efficiency (η_{tr}) and charge separation efficiency (η_{sep}) of CoPOM-containing electrodes under different applied potentials d).

increased in the presence of both CN_x sensitizer and CoPOM cocatalyst. Importantly, the polymeric PEI linker-containing CoPOM-PEI-CN_x-TiO_2 photoanode showed the highest photocurrents within the whole potential range and also the highest monochromatic quantum efficiencies (IPCE) measured at a constant bias potential of 1.12 V versus RHE (Figure 2b). Importantly, the CoPOM-PEI-CN_x-TiO_2 photoanode exhibited also the most negative photocurrent onset potential of 0.2 V versus RHE, which clearly indicates an improved rectifying behavior due to more effective extraction of photogenerated holes from CN_x. Figure 2c shows photocurrent transients under the same visible light irradiation conditions at a constant potential of 0.78 V versus RHE, and indicates a relatively good short-term stability of the photocurrent response. Interestingly, for the CoPOM-free electrode (black line), the current spikes after switching on the light and negative current overshoots appearing after the light is switched off become significantly more pronounced. Such spikes and overshoots are a typical fingerprint of intense surface recombination processes,[58] indicating that, in the absence of water oxidation catalyst, the photoholes in CN_x do not undergo the desired interfacial transfer, but instead accumulate in the CN_x layer and subsequently either recombine or induce photocorrosion. In contrast, the current spikes are less pronounced and the overshoots are nearly absent in both CoPOM-containing electrodes, which again indicates that the CoPOM cocatalyst can extract holes generated in the CN_x layer and trigger the desired water oxidation reaction.

In order to shed more light on the factors governing the photoresponse of CoPOM-containing photoanodes, we performed an analysis of charge separation (η_{sep}) and hole transfer (η_{tr}) efficiencies according to established protocols.[49,50,59] This analysis is based on the assumption that the measured photocurrent density in water oxidation can be calculated by multiplying the maximum possible photocurrent (obtained from the absorbed photon flux) by η_{sep} and η_{tr}, whereby the hole transfer efficiency η_{tr} in the presence of a readily oxidizable reducing agent (here Na_2SO_3) is taken as 100%; for details see the experimental section. The calculated η_{tr} and η_{sep} values for the both CoPOM-containing electrodes are depicted in Figure 2d, calculated from data in Figure 2a and Figure S8 (Supporting Information). As expected, both efficiencies show clear dependence on the applied potential as stronger positive applied bias is beneficial for both charge separation and hole transfer. Notably, the charge separation efficiency η_{sep} is very similar for both PEI linker-free CoPOM-CN_x-TiO_2 and PEI-containing CoPOM-PEI-CN_x-TiO_2, which is also in line with only minor differences in PL spectra of the corresponding photoanodes that are possibly related to slightly more efficient quenching of emissive states in CN_x (Figure S9, Supporting Information). In stark contrast, the CoPOM-PEI-CN_x-TiO_2 exhibits significantly higher charge transfer efficiencies than CoPOM-CN_x-TiO_2 in the whole potential range. In other words, these data suggest that the superior photoelectrocatalytic behavior of the PEI linker-containing CoPOM-PEI-CN_x-TiO_2 photoanode arises from a more efficient

© 2022 The Authors. Advanced Sustainable Systems published by Wiley-VCH GmbH

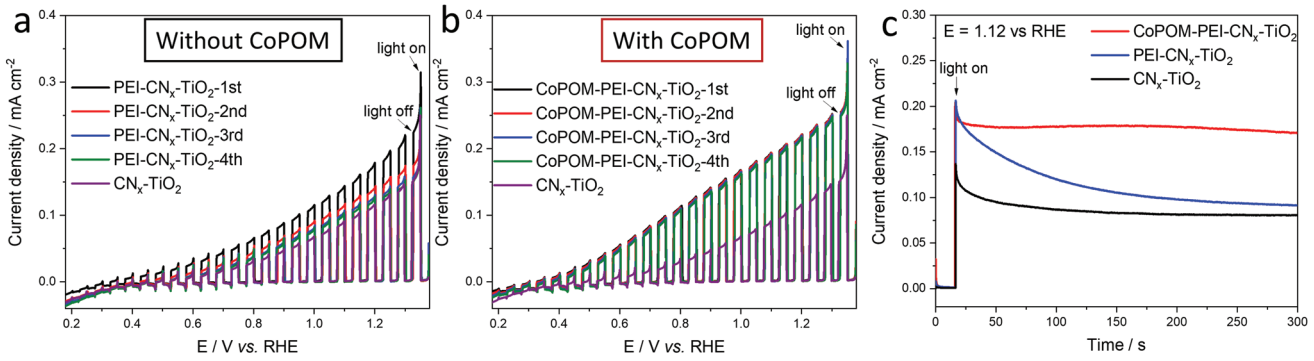

Figure 3. Photocurrent stability test recorded under intermittent polychromatic irradiation ($\lambda > 420$ nm, 150 mW cm^{-2}) in a borate electrolyte (0.1 M, pH 8) at cathodic sweep of 5 mV s^{-1} for photoanode with a) and without b) the CoPOM cocatalyst; chronoamperometric curves under illumination showing the degradation of PEI in the absence of CoPOM c).

transfer of photogenerated holes from CN_x to water, which can be attributed to the higher CoPOM loading due to the beneficial effect of the cationic PEI polymer linker.

However, in addition to its beneficial effect on the CoPOM immobilization, a question arises whether the cationic PEI polymer could potentially also act as a sacrificial electron donor that can be simply more easily oxidized than water by holes from CN_x. In order to directly address this issue, we measured the photocurrents from the CN_x-TiO_2 electrode modified with PEI polymer only (dipped in PEI solution five times), and the measurements at PEI-CN_x-TiO_2 photoanodes were repeated subsequently in four cycles. The deposition of PEI enhanced photocurrents, but a gradual decrease of photocurrents was observed, ending up at the same values as those for the CN_x-TiO_2 photoanode (**Figure 3**a). Hence, in the absence of the CoPOM catalyst, the PEI does effectively extract the holes from CN_x, but is thereby oxidatively degraded. As a next step, the same protocol was also applied to the CoPOM-PEI-CN_x-TiO_2 photoanode. Contrary to the gradual decline of photocurrents observed for PEI-CN_x-TiO_2, the photocurrents at CoPOM-PEI-CN_x-TiO_2 remain completely stable over all four cycles (Figure 3b). This is also in line with the chronoamperometric photocurrent measurements of the three electrodes (Figure 3c), which show that PEI-CN_x-TiO_2 exhibits a fast decline in photocurrent due to degradation of PEI in the absence of CoPOM, whereby the photocurrent at CoPOM-PEI-CN_x-TiO_2 is practically stable. Therefore, we conclude that in the presence of CoPOM, the holes are efficiently transferred from PEI to the CoPOM catalyst where they drive water oxidation, and the cationic PEI linker is thereby effectively stabilized.

In order to unambiguously prove the dioxygen evolution at CoPOM modified photoanodes, we performed photoelectrocatalytic OER measurements (**Figure 4**a) in a borate solution (pH 8) under prolonged (1 h) visible light irradiation ($\lambda > 420$ nm, 150 mW cm^{-2}). Both CoPOM-containing hybrid photoanodes, CoPOM-CN_x-TiO_2 and CoPOM-PEI-CN_x-TiO_2, clearly exhibit OER activity under visible light illumination. This confirms our assumption that charge transfer from CN_x to CoPOM is feasible and that the presence of the CoPOM cocatalyst is necessary to trigger the OER. Importantly, at the PEI-containing electrode the oxygen evolution rate was doubled compared to the counterpart photoanode without PEI. Importantly, no oxygen evolution was observed at the CoPOM-free CN_x-TiO_2 photoanode despite substantial photocurrents that can be ascribed to photocorrosion.[38] This result is also in line with our previous studies that confirmed that the presence of an effective OER catalyst is absolutely necessary to observe oxygen as a product of water oxidation at CN_x–TiO_2 hybrid photoanodes.[26,34–41] On the other hand,

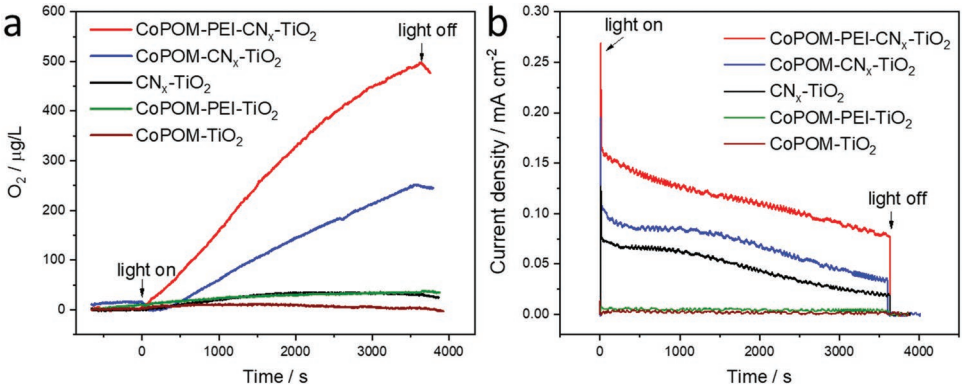

Figure 4. Dioxygen evolution a) and corresponding photocurrent transients b); measured under polychromatic visible light irradiation ($\lambda > 420$ nm, 150 mW cm^{-2}) at 1.12 V versus RHE in a borate electrolyte (0.1 M, pH 8.0). The oxygen evolution was measured at least at three different electrodes (representative curves are shown), and the error is taken as 2σ (σ = standard deviation; 95% confidence interval).

© 2022 The Authors. Advanced Sustainable Systems published by Wiley-VCH GmbH

CN_x-free pristine TiO_2 photoanodes modified with CoPOM exhibited neither photocurrents nor oxygen evolution since pristine TiO_2 does not absorb in the visible range. The apparent (based on dissolved O_2 and uncorrected for losses in the headspace) Faradaic efficiencies (FE) of oxygen evolution for CoPOM-PEI-CN_x-TiO_2 (15% ± 4%) and for CoPOM-CN_x-TiO_2 (12% ± 4%) are rather low, which suggests that even in the best photoanodes the overall utilization of holes generated in CN_x for water oxidation is still far from optimum, and a substantial portion of holes does not induce the OER but instead contributes to the photocorrosion of CN_x (Figure 4b). The improved photocurrent onset potential, higher oxygen production rate, and FE at the PEI-containing CoPOM-PEI-CN_x-TiO_2 photoanode clearly confirm the beneficial effect of the cationic PEI polymer that serves as an effective linker by establishing the electrostatic attraction between the CN_x sensitizer and CoPOM catalyst that are both negatively charged. This results in a more efficient hole extraction from CN_x and more effective utilization of photogenerated holes for water oxidation due to the more effective immobilization (i.e., higher loading) of the CoPOM water oxidation catalyst.

4. Conclusion

For the first time, a triad photoanode comprising a molecular cobalt polyoxometalate (CoPOM) embedded in the porous structure of hybrid photoanodes consisting of polymeric carbon nitride deposited onto an electron collecting porous TiO_2 layer is reported. The photoanodes exhibit complete water oxidation to dioxygen under visible (λ > 420 nm) light irradiation, with photocurrents down to relatively low bias potentials of 0.2 V versus RHE. Importantly, it is demonstrated that PEI, a positively charged cationic polymer that has been previously reported to enable improved deposition of CoPOM onto various metal oxides,[47,48,60] can also act as a highly effective electrostatic linker for immobilization of the anionic CoPOM onto the negatively charged surface of carbon nitride. Mechanistic studies revealed that the optimized deposition of CoPOM using the PEI linker translates directly into improved efficiency of the transfer of photogenerated oxidizing equivalents (holes) to water molecules and thus to enhanced oxygen evolution. On the other hand, the charge separation efficiency in triad photoanodes was largely unaffected by the CoPOM loading, and remained rather low (below 10% at moderate bias potentials), suggesting that primary recombination is a key performance bottleneck in triad photoanodes. Importantly, we also show that the PEI linker is effectively stabilized in the presence of the CoPOM catalyst that efficiently extracts the holes from PEI, preventing thus the oxidative degradation that takes place in the absence of CoPOM. This work thus highlights the importance of careful design of multi-component photoelectrocatalytic systems, and provides a simple protocol for effective immobilization of POM-based catalysts into soft matter-based photoelectrocatalytic architectures for light-driven water oxidation.

Supporting Information

Supporting Information is available from the Wiley Online Library or from the author.

Acknowledgements

This work was funded by the Deutsche Forschungsgemeinschaft (DFG, German Research Foundation) – Project number 364549901–TRR 234 CataLight (Projects B6, B2, C4). The authors thank Joachim Bansmann for his help with XPS analysis and Hanna Braun for her help with electrochemical investigation. R.G. and S.R. acknowledge the financial support from the Vector Stiftung.

Open access funding enabled and organized by Projekt DEAL.

Conflict of Interest

The authors declare no conflict of interest.

Data Availability Statement

The data that support the findings of this study are available from the corresponding author upon reasonable request.

Keywords

carbon nitride, oxygen evolution, photoelectrochemistry, polyoxometalates, water splitting

Received: November 26, 2021
Revised: February 9, 2022
Published online: March 8, 2022

[1] T. Hisatomi, J. Kubota, K. Domen, *Chem. Soc. Rev.* **2014**, *43*, 7520.
[2] Y. Wang, H. Suzuki, J. Xie, O. Tomita, D. J. Martin, M. Higashi, D. Kong, R. Abe, J. Tang, *Chem. Rev.* **2018**, *118*, 5201.
[3] S. Chen, T. Takata, K. Domen, *Nat. Rev. Mater.* **2017**, *2*, 17050.
[4] X. Li, J. Yu, J. Low, Y. Fang, J. Xiao, X. Chen, *J. Mater. Chem. A* **2015**, *3*, 2485.
[5] S. J. A. Moniz, S. A. Shevlin, D. J. Martin, Z. X. Guo, J. Tang, *Energy Environ. Sci.* **2015**, *8*, 731.
[6] X. Wang, K. Maeda, A. Thomas, K. Takanabe, G. Xin, J. M. Carlsson, K. Domen, M. Antonietti, *Nat. Mater.* **2009**, *8*, 76.
[7] F. K. Kessler, Y. Zheng, D. Schwarz, C. Merschjann, W. Schnick, X. Wang, M. J. Bojdys, *Nat. Rev. Mater.* **2017**, *2*, 17030.
[8] X. Li, Z. Cheng, Y. Fang, X. Fu, X. Wang, *Sol. RRL* **2020**, *4*, 2000168.
[9] H. Zhang, W. Tian, X. Duan, H. Sun, Y. Shen, G. Shao, S. Wang, *Nanoscale* **2020**, *12*, 6937.
[10] D. J. Martin, P. J. T. Reardon, S. J. A. Moniz, J. Tang, *J. Am. Chem. Soc.* **2014**, *136*, 12568.
[11] D. J. Martin, K. Qiu, S. A. Shevlin, A. D. Handoko, X. Chen, Z. Guo, J. Tang, *Angew. Chem., Int. Ed.* **2014**, *53*, 9240.
[12] G. Liu, T. Wang, H. Zhang, X. Meng, D. Hao, K. Chang, P. Li, T. Kako, J. Ye, *Angew. Chemie* **2015**, *127*, 13765.
[13] M. Zhu, S. Kim, L. Mao, M. Fujitsuka, J. Zhang, X. Wang, T. Majima, *J. Am. Chem. Soc.* **2017**, *139*, 13234.
[14] A. Rajagopal, E. Akbarzadeh, C. Li, D. Mitoraj, I. Krivtsov, C. Adler, T. Diemant, J. Biskupek, U. Kaiser, C. Im, M. Heiland, T. Jacob, C. Streb, B. Dietzek, R. Beranek, *Sustain. Energy Fuels* **2020**, *4*, 6085.
[15] G. Gao, Y. Jiao, E. R. Waclawik, A. Du, *J. Am. Chem. Soc.* **2016**, *138*, 6292.
[16] G. Zhao, H. Pang, G. Liu, P. Li, H. Liu, H. Zhang, L. Shi, J. Ye, *Appl. Catal. B Environ.* **2017**, *200*, 141.
[17] Y. Shiraishi, S. Kanazawa, Y. Sugano, D. Tsukamoto, H. Sakamoto, S. Ichikawa, T. Hirai, *ACS Catal.* **2014**, *4*, 774.

© 2022 The Authors. Advanced Sustainable Systems published by Wiley-VCH GmbH

[18] A. Savateev, I. Ghosh, B. König, M. Antonietti, *Angew. Chemie – Int. Ed.* **2018**, *57*, 15936.
[19] I. Ghosh, J. Khamrai, A. Savateev, N. Shlapakov, M. Antonietti, B. König, *Science* **2019**, *365*, 360.
[20] I. Krivtsov, D. Mitoraj, C. Adler, M. Ilkaeva, M. Sardo, L. Mafra, C. Neumann, A. Turchanin, C. Li, B. Dietzek, R. Leiter, J. Biskupek, U. Kaiser, C. Im, B. Kirchhoff, T. Jacob, R. Beranek, *Angew. Chemie – Int. Ed.* **2020**, *59*, 487.
[21] M. Wei, L. Gao, J. Li, J. Fang, W. Cai, X. Li, A. Xu, *J. Hazard. Mater.* **2016**, *316*, 60.
[22] C. Zhou, G. Zeng, D. Huang, Y. Luo, M. Cheng, Y. Liu, W. Xiong, Y. Yang, B. Song, W. Wang, *J. Hazard. Mater.* **2020**, *386*, 121947.
[23] J. T. Kirner, R. G. Finke, *J. Mater. Chem. A* **2017**, *5*, 19560.
[24] M. N. Collomb, D. V. Morales, C. N. Astudillo, B. Dautreppe, J. Fortage, *Sustain. Energy Fuels* **2019**, *4*, 31.
[25] D. G. Nocera, *Acc. Chem. Res.* **2017**, *50*, 616.
[26] L. Wang, D. Mitoraj, S. Turner, O. V. Khavryuchenko, T. Jacob, R. K. Hocking, R. Beranek, *ACS Catal.* **2017**, *7*, 4759.
[27] C. Adler, I. Krivtsov, D. Mitoraj, L. dos Santos-Gómez, S. García-Granda, C. Neumann, J. Kund, C. Kranz, B. Mizaikoff, A. Turchanin, R. Beranek, *ChemSusChem* **2021**, *14*, 2170.
[28] C. Adler, S. Selim, I. Krivtsov, C. Li, D. Mitoraj, B. Dietzek, J. R. Durrant, R. Beranek, *Adv. Funct. Mater.* **2021**, *31*, 2105369.
[29] H. Ou, P. Yang, L. Lin, M. Anpo, X. Wang, *Angew. Chemie – Int. Ed.* **2017**, *56*, 10905.
[30] F. Podjaski, J. Kröger, B. V. Lotsch, *Adv. Mater.* **2018**, *30*, 1705477.
[31] J. Qin, J. Barrio, G. Peng, J. Tzadikov, L. Abisdris, M. Volokh, M. Shalom, *Nat. Commun.* **2020**, *11*, 4701.
[32] N. Karjule, J. Barrio, L. Xing, M. Volokh, M. Shalom, *Nano Lett.* **2020**, *20*, 4618.
[33] M. Shalom, S. Gimenez, F. Schipper, I. Herraiz-Cardona, J. Bisquert, M. Antonietti, *Angew. Chemie* **2014**, *126*, 3728.
[34] L. Wang, M. Bledowski, A. Ramakrishnan, D. König, A. Ludwig, R. Beranek, *J. Electrochem. Soc.* **2012**, *159*, H616.
[35] M. Bledowski, L. Wang, A. Ramakrishnan, A. Bétard, O. V. Khavryuchenko, R. Beranek, *ChemPhysChem* **2012**, *13*, 3018.
[36] M. Bledowski, L. Wang, A. Ramakrishnan, R. Beranek, *J. Mater. Res.* **2013**, *28*, 411.
[37] B. Mei, H. Byford, M. Bledowski, L. Wang, J. Strunk, M. Muhler, R. Beranek, *Sol. Energy Mater. Sol. Cells* **2013**, *117*, 48.
[38] M. Bledowski, L. Wang, S. Neubert, D. Mitoraj, R. Beranek, *J. Phys. Chem. C* **2014**, *118*, 18951.
[39] O. V. Khavryuchenko, L. Wang, D. Mitoraj, G. H. Peslherbe, R. Beranek, *J. Coord. Chem.* **2015**, *68*, 3317.
[40] P. Longchin, D. Mitoraj, O. M. Reyes, C. Adler, N. Wetchakun, R. Beranek, *JPhys Energy* **2020**, *2*, 044001.
[41] R. Gong, D. Mitoraj, R. Leiter, M. Mundszinger, A. K. Mengele, I. Krivtsov, J. Biskupek, U. Kaiser, R. Beranek, S. Rau, *Front. Chem.* **2021**, *9*, 593.
[42] Q. Yin, J. M. Tan, C. Besson, Y. V. Geletii, D. G. Musaev, A. E. Kuznetsov, Z. Luo, K. I. Hardcastle, C. L. Hill, *Science* **2010**, *328*, 342.
[43] M. Natali, S. Berardi, A. Sartorel, M. Bonchio, S. Campagna, F. Scandola, *Chem. Commun.* **2012**, *48*, 8808.
[44] J. W. Vickers, H. Lv, J. M. Sumliner, G. Zhu, Z. Luo, D. G. Musaev, Y. V. Geletii, C. L. Hill, *J. Am. Chem. Soc.* **2013**, *135*, 14110.
[45] J. J. Stracke, R. G. Finke, *ACS Catal.* **2013**, *3*, 1209.
[46] J. J. Stracke, R. G. Finke, *ACS Catal.* **2014**, *4*, 79.
[47] D. Jeon, H. Kim, C. Lee, Y. Han, M. Gu, B. S. Kim, J. Ryu, *ACS Appl. Mater. Interfaces* **2017**, *9*, 40151.
[48] Y. Han, K. Choi, H. Oh, C. Kim, D. Jeon, C. Lee, J. H. Lee, J. Ryu, *J. Catal.* **2018**, *367*, 212.
[49] H. Dotan, K. Sivula, M. Grätzel, A. Rothschild, S. C. Warren, *Energy Environ. Sci.* **2011**, *4*, 958.
[50] Y. Gao, T. W. Hamann, *Chem. Commun.* **2017**, *53*, 1285.
[51] (ASTM) G-173 spectra, https://www.nrel.gov/grid/solar-resource/spectra-am1.5.html.
[52] Y. Zhang, A. Thomas, M. Antonietti, X. Wang, *J. Am. Chem. Soc.* **2009**, *131*, 50.
[53] F. Guo, Y. Hou, A. M. Asiri, X. Wang, *Chem. Commun.* **2017**, *53*, 13221.
[54] R. Mészáros, L. Thompson, M. Bos, P. De Groot, *Langmuir* **2002**, *18*, 6164.
[55] M. Bledowski, L. Wang, A. Ramakrishnan, O. V. Khavryuchenko, V. D. Khavryuchenko, P. C. Ricci, J. Strunk, T. Cremer, C. Kolbeck, R. Beranek, *Phys. Chem. Chem. Phys.* **2011**, *13*, 21511.
[56] P. Makuła, M. Pacia, W. Macyk, *J. Phys. Chem. Lett.* **2018**, *9*, 6814.
[57] I. S. Cho, Z. Chen, A. J. Forman, D. R. Kim, P. M. Rao, T. F. Jaramillo, X. Zheng, *Nano Lett.* **2011**, *11*, 4978.
[58] L. M. Peter, *Chem. Rev.* **1990**, *90*, 753.
[59] F. F. Abdi, A. Chemseddine, S. P. Berglund, R. Van De Krol, *J. Phys. Chem. C* **2017**, *121*, 153.
[60] R. Gong, D. Gao, R. Liu, D. Sorsche, J. Biskupek, U. Kaiser, S. Rau, C. Streb, *ACS Appl. Energy Mater.* **2021**, *4*, 12671.

© 2022 The Authors. Advanced Sustainable Systems published by Wiley-VCH GmbH